

Effect of inter-segmental air exchanges on local and overall clothing ventilation

Nagham Ismail, Nesreen Ghaddar and Kamel Ghali

Textile Research Journal
2016, Vol. 86(4) 423–439
© The Author(s) 2016
Reprints and permissions:
sagepub.co.uk/journalsPermissions.nav
DOI: 10.1177/00405175155591775
trj.sagepub.com



Abstract

The aim of this work is to study the effect of the connection between arm and trunk segments in changing the flow characteristics and local ventilation. A model is developed that solves coupled momentum, mass and heat balances, including buoyancy for the connected clothed upper human body. The model was validated by performing computational fluid dynamics simulations to compare the microclimate air flow characteristics and flow direction at the connections. In addition, the model was also validated by comparing predicted overall ventilation with published data.

The interconnection air exchanges affected significantly local ventilation in the trunk segment and the direction of the flow in the open-aperture-clothed arm segment. It was found that at relatively high wind speed ($V_w \geq 0.9$ m/s) and with a permeable jacket, the inter-segmental ventilation became important and exceeded 5 l/min. Meanwhile, this inter-segmental ventilation caused an increase of 15% of trunk ventilation and a reduction of 4% of arm ventilation. The inter-segmental ventilation vanished and the air exchange between the trunk and the arm was no longer important at low permeability ($\alpha = 0.05$ m/s) and at low wind speed ($V_w = 0.1$ m/s). Finally, the inter-segmental ventilation was more important for the open clothed arm aperture compared to when it was closed.

Keywords

clothing inter-segmental air exchanges, local clothing ventilation, modeling microclimate ventilation

Over the years, researchers have been interested in measuring local ventilation of human body through clothing. Clothing ventilation is an effective way for the human body to lose heat in hot environments.¹ Most literature research focused on experimentally measuring ventilation using the trace gas dilution method^{1–3} and reported the average ventilation value for the clothed body surface area. Available experimental data on clothing ventilation were mainly for whole ensemble or for independent unconnected segments.^{4–8}

Predicting segmental clothing ventilation is important for improving garment design by modifying design parameters to enhance or decrease the local ventilation rate depending on the type of clothing, including protective clothing. This is why researchers have been interested in developing mathematical models from the first principles to predict local clothing ventilation. The modeling approach has mainly been based on representing the human body as a number of independent cylindrical segments covered with garment material in cross air flow.^{7–10} Each clothed segment is formed by an inner cylinder representing the body skin

and the outer cylinder representing the clothed garment. The segmental skin temperature is predicted from a finite element model of human thermal physiology, such as a bioheat model,^{6,11} and is set as the boundary condition for the ventilation model. Clothed cylinder models mimicked a limb or a trunk and the overall ventilation rate of an ensemble was obtained by summing the segmental ventilation rates.⁶ However, these methods assume that segments are not connected and there is no air that flows from one segment to another, which is not the case in real physical

Department of Mechanical Engineering, Faculty of Engineering and Architecture, American University of Beirut, Lebanon

Corresponding author:

Nesreen Ghaddar, Associate Provost & Qatar Chair in Energy Studies Professor, Department of Mechanical Engineering, American University of Beirut, P.O. Box 11-236, Riad El Solh, Beirut 1107 2020, Lebanon.
Email: farah@aub.edu.lb

situations. Indeed, Ke et al.¹ prescribed the microclimate ventilation as the air exchange between a specific garment and the environment, including three parts: air exchange between local body parts' microclimates, air exchange through the fabric with the environment, and air exchange through garment apertures with the environment. Despite the fact that ventilation includes these three processes, research focused on the effect of air exchange through fabric³ and air exchange through garment apertures.^{3,6} The ventilation through fabric is studied by modeling the flow characteristics of air penetrating through a permeable jacket or by finding the overall ventilation rate experimentally by using a permeable jacket without evaluating the segmental ventilation rate.⁴ Furthermore, the ventilation through garment apertures with the environment was predicted empirically by experimentation where the garment used is usually impermeable and the connections between segments were closed.¹ However, to the author's knowledge, no published experimental or analytical work has examined the impact of the air exchange between local parts on the flow characteristics of air and on the segmental ventilation rate. The studying of air flow across annular segmental connection is important when considering protective clothing design. In fact, some contaminants and toxic particles adhere with air and are transported with it. For instance, toxic aerosol particles handled by air can enter the arm from its bottom opening and can be transported upward toward the connection with the trunk. Therefore, the novelty of this work arises from studying the impact of body segment connections on the air flow characteristics in the microclimate layer and thus on estimating local ventilation rates.

In this work, the coupled mass, momentum, and heat balances, including buoyancy effect, are solved for the upper human body formed by three connected cylinders in a cross-wind. The flow over side-by-side cylinders of different diameters in cross-flow for the upper trunk connection with the arm was modeled as a single cylinder. The segmental skin temperature used as the boundary condition is considered constant. The predicted flow characteristics and segmental ventilation rates were respectively validated by three-dimensional (3D) computational fluid dynamics (CFD) analysis and by published experiments. The flow in the microclimate annuli of the trunk, sleeves, and connection is simulated using the commercial software ANSYS Fluent to validate the segmental ventilation predicted by the model. In addition, segmental ventilation rates are summed and validated with published experimental overall ventilation data. A parametric study was followed to determine the design factors that enhance inter-segmental ventilation between the clothed trunk and arm.

Mathematical formulation

Fabric-covered cylinders provide a convenient geometry to provide the physical representation of clothed human body segments subject to cross-wind. However, the upper body connection through the shoulders needs to be incorporated as a connecting geometry for the microclimate air flow between the arm and trunk segments. The physical model is shown in Figures 1 and 2, where the upper human body part is assumed to be symmetrical and is subject to external relative cross-wind. The physical model is divided into four annular zones, Z1, Z2, Z3, and Z4, associated with the lower human clothed arm, the upper clothed arm, the clothed trunk, and the clothed shoulder part, respectively (Figures 1 and 2).

Forced convection around the two adjacent vertical clothed cylinders is studied according to the spacing between them. When air penetrates into clothing, it is going to flow in angular and axial directions in the air annulus separating the inner heated cylinder and the clothing. However, because of the temperature difference between the skin and the inner cylinder, natural convection also plays an important role in the air flow characteristics, besides the forced convection.^{6,12,13} Mixed convection will then be studied by solving the mass, momentum, and heat balances of the microclimate air annuli. The mathematical model predicts the impact of the connection between segments on the flow characteristics.

To assess the impact of the segmental connections on the flow characteristics, a 3D detailed CFD model is also developed using ANSYS Fluent 14.5.¹⁴ The aim of the CFD model is to investigate the flow of air in the microclimate air layer between the skin and the clothing and particularly in the interconnection region. The skin temperature is held constant and the flow characteristics will be used to validate the simplified mathematical model at isothermal skin temperature.

The ventilation rates of the connected segments are compared with published experiments that aim to find the overall ventilation rates through ensembles where the connections between segments are left open.^{3,15}

Clothed upper human body simplified mathematical model

External wind flow and clothed body representation

In order to model the heat and moisture transfer of the upper part of the human body, it is important to understand the external flow field around the two adjacent vertical and clothed cylinders (see Figures 1 and 2). Forced convection around side-by-side circular cylinders of the same diameter is studied thoroughly in the

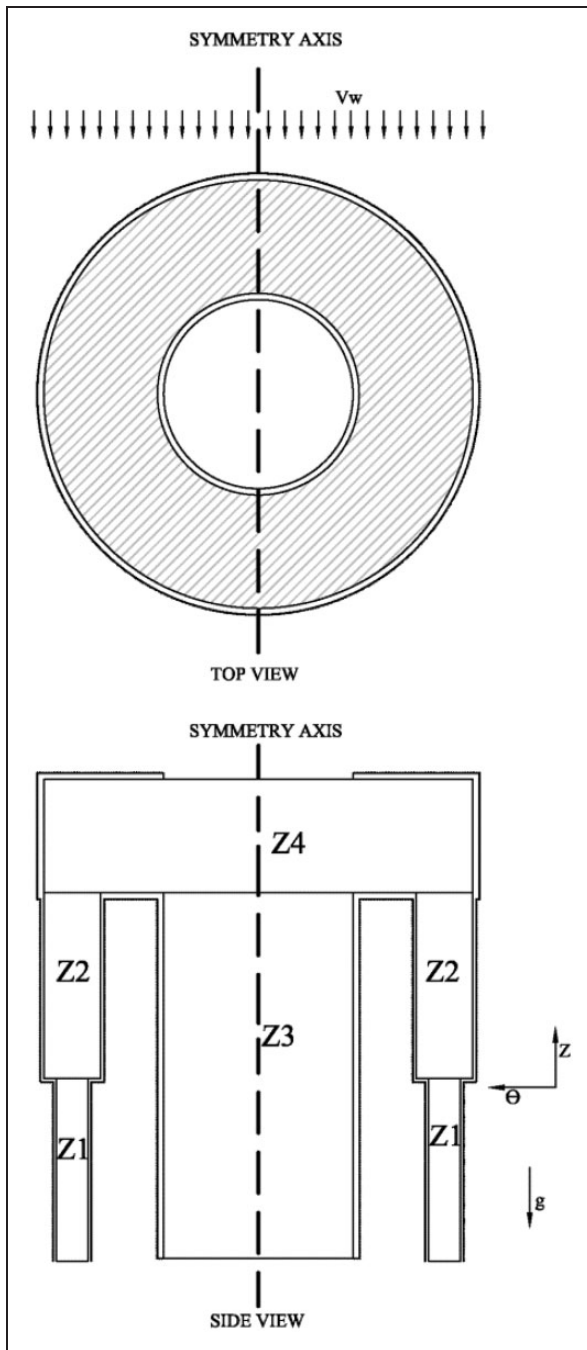


Figure 1. Physical configuration of the upper part of the human body.

literature.¹⁶⁻¹⁹ However, the human arm and human trunk present cylinders with different diameters with a diameter ratio of 0.25 between the small cylinder and the large one.

Although few studies in the literature discuss the flow past two circular diameters of different diameters,^{20,21} a numerical simulation of viscous flow past two circular cylinders of different diameters with similar diameter ratio was reported by Zhao and Yan²²

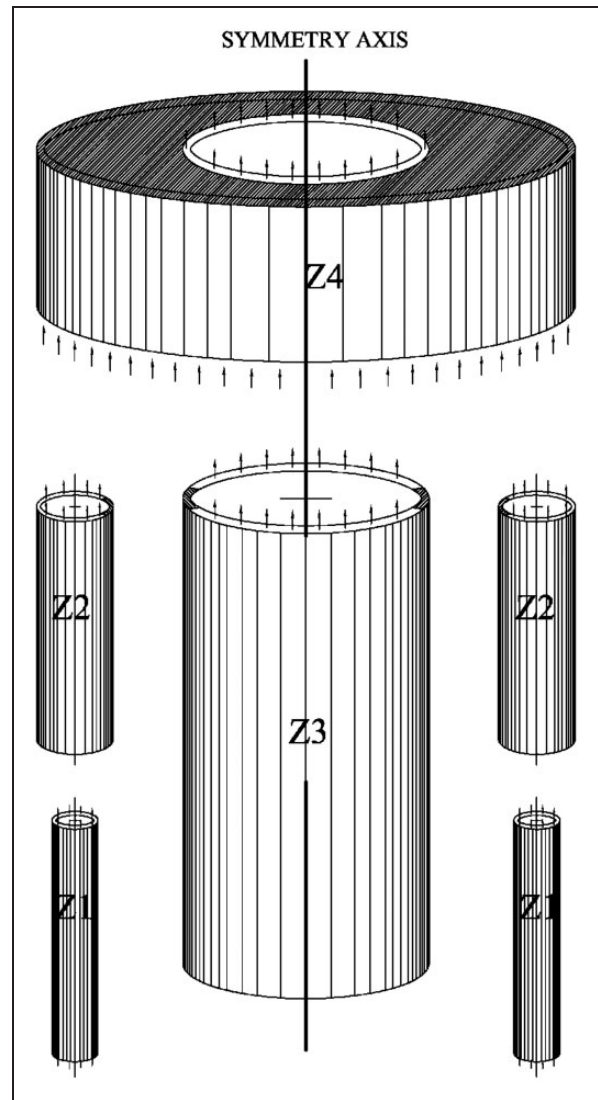


Figure 2. Blow up of the clothed segments.

In their work, the diameter ratio between the small cylinder and the large one was also 0.25. The gap between the small cylinder and the large cylinder ranged from 0.05 to 1.0 times the diameter of the large cylinder. They concluded that the flow behind the two cylinders can be classified into three types;²² for the very small gap ratio, there is only one wake behind the two cylinders so they are considered as a bluff single body; for the medium gap ratios, the interaction mode occurs: strong interactions exist between the vortex shedding from the large cylinder and the shedding from the small cylinder; and for very large gap ratios, the interaction between the shedding from the two cylinders becomes very weak, thus the cylinders are considered as independent cylinders. According to finding of Zhao and Yan,²² the flow over the arms and the trunk depended on the height considered. The gap

between the small cylinder and the large cylinder ranges from 1/12 above the shoulder level to 2/3 below the shoulder level times the diameter of the large cylinder (Figures 1 and 2). Therefore, the flow is considered similar to the flow around a single bluff body above the shoulder level and similar to the flow around independent cylinders below the shoulder level. For this reason, one large cylinder represents the two arms and the trunk above the shoulder level, and three independent cylinders extend downward from the large cylinder (Figures 1 and 2). Each of the arms and the trunk is formed by two co-axial annuli of different inner and outer radii. The inner solid cylinder represents the heated skin and an outer cylinder represents the permeable fabric. The two cylinders are separated by a few millimeters of microclimate air annulus where the flow and heat characteristics are modeled and studied.

Adopted fabric model

The outer clothing cylinder is assumed to consist of a layer of fibers containing air voids. Air penetrates fabric through pores and enters the microclimate space between skin and clothing. Water vapor is assumed to diffuse through the air void space to be absorbed or desorbed by fibers, depending on the type of fabric. In order to accurately model the fabric, we adopt the model of Ghali et al.,²³ which divided the fabric into three nodes: the void node representing the air within the fabric; the outer node that is exposed to ambient conditions, air in the void node, and in microclimate air layer; and the inner node surrounded by the outer node. This modeling from first principles captured the heat and moisture transport in fabrics as detailed in the literature.^{5,9,24} Note that the fabric three-node model lumped fabric into outer, inner and air void nodes. The outer node is in direct contact with the penetrating air in the void space (air void node); the inner node represented the inner portion of the solid yarn, surrounded by the fabric outer node and exchanging heat and moisture transfer by diffusion only with the outer node. The outer node exchanges heat and moisture transfer with the flowing air in the air void node and with the inner node. However, volume changes of fibers due to the sorption process are small enough and can be neglected.²³ In addition, the water vapor is assumed to dilute in the air mixture.

In this work, skin is assumed to be exchanging heat and moisture with the microclimate air layer and radiation heat transfer with the outer node. Thus, skin is considered as an interface so that there is no storage term (transient term) to be considered. As in previous researches, fully developed Poiseuille flow in both angular and axial directions was used⁶ due to the small microclimate air annuli thickness, which reduces the

mathematical model to a one-dimensional (1D) flow problem in two directions (angular and axial), while the radial direction is lumped.

Heat and mass transport in air annulus sheathed by porous fabric

The mass, momentum, and energy balances are presented for the thin microclimate air layer trapped between the skin and clothing while taking into consideration the lumped flow in the radial direction. The mathematical formulation will be based on the coupled pressure equation of mass and momentum for narrow annular flow reported in the previous work¹² that assumes fully developed Poiseuille flow in the horizontal angular direction and fully developed mixed buoyant upward flow.^{7,9} With these assumptions and under conditions of incompressible Boussinesq fluid of constant thermo-physical properties, the formulation of the 3D problem of the coupled momentum and heat transfer in the vertical annulus is transformed into the 1D problem of coupled energy balance and pressure equation derived from mass and momentum equations:¹⁰

The pressure equation for the annular air flow¹² is the given by

$$\frac{\alpha \rho_{ma}(P_{mc} - P_s)}{\Delta P_m} + \frac{\partial}{R_f^2 \partial \theta} \left(\frac{Y^3}{12\nu} \frac{\partial P_{mc}}{\partial \theta} \right) + \frac{\partial}{\partial z} \left(\frac{Y^3}{12\nu} \frac{\partial P_{mc}^*}{\partial z} \right) - \rho_{mc} \frac{g\beta Y^2}{12\nu} (T_{mc} - T_{void}) = 0 \quad (1a)$$

where α is the fabric air permeability expressed in m/s tested at a pressure drop $\Delta P_m = 0.1245$ kPa from standard tests on fabric air permeability, P_{mc} is the air pressure in the microclimate trapped air layer (kPa), P_s is the external adjacent air layer pressure (kPa) assumed to be the same pressure distribution around a solid cylinder at flow condition V_w , T_{mc} is the air temperature in the microclimate trapped air layer ($^{\circ}\text{C}$), and T_{void} is the air temperature in the void node ($^{\circ}\text{C}$). The first term of Equation (1) is the radial penetrating air flow rate per unit area over the air density. The second term is the net mass flow rate in the angular direction assuming a Poiseuille flow model in this direction over the air density. The third term is the net axial mass flow rate induced by the forced flow due to driving pressure and by the natural convection due to temperature gradient²⁵ over the air density.

The water vapor transport in the microclimate air annulus is given by

$$h_{m(s-a)}(P_{v-skin} - P_{v-mc}) + h_{m(o-a)}(P_{v-o} - P_{v-mc}) + \max(\dot{m}_{ay}, 0)w_{void} - \max(-\dot{m}_{ay}, 0)w_{mc}$$

$$\begin{aligned}
& -\frac{\partial}{\partial z}(\dot{m}_{az} Y w_{mc}) - \frac{\partial}{R_f \partial \theta}(\dot{m}_{a\theta} Y w_{mc}) \\
& + D Y \rho_{mc} \frac{\partial^2 w_{mc}}{\partial z^2} + D Y \rho_{mc} \frac{\partial^2 w_{mc}}{R_f^2 \partial \theta^2} \\
& + D \rho_{mc} \frac{(w_{void} - w_{mc})}{ef/2} = 0
\end{aligned} \quad (1b)$$

where $h_{m(s-a)}$ is the mass transfer coefficient between skin and air, P_{v-skin} is the partial pressure of the skin vapor pressure (kPa), P_{v-a} is the partial pressure of the air vapor pressure (kPa), $h_{m(o-a)}$ is the mass transfer coefficient between the outer fabric node and air, P_{v-o} is the partial pressure of the outer node vapor pressure (kPa), P_{v-o} is the partial pressure of the outer node vapor pressure (kPa), w_{void} is the humidity ratio of the void node, and w_a is the humidity ratio of the air layer.

The steady-state energy balance on the microclimate air layer is a balance of the convective heat and mass transfer due to the flow of air in the axial, angular, and radial directions, the evaporative heat transfer from the surface of the inner cylinder representing the skin, the heat and mass diffusion from void air of the thin fabric to the air layer, and the axial and angular conduction of heat in the air layer. Thus, the energy balance in the microclimate air layer is given by

$$\begin{aligned}
& h_{m(s-a)} h_{fg} (P_{v-skin} - P_{v-mc}) + h_{m(o-a)} h_{fg} (P_{v-o} - P_{v-mc}) \\
& + \max(\dot{m}_{ay}, 0) (w_{void} + c_p T_{void}) - \max(-\dot{m}_{ay}, 0) \\
& \times (w_{mc} + c_p T_{mc}) - \frac{\partial}{\partial z}(\dot{m}_{az} Y (w_{mc} h_{fg} + c_p T_{mc})) \\
& - \frac{\partial}{R_f \partial \theta}(\dot{m}_{a\theta} Y (w_{mc} h_{fg} + c_p T_{mc})) + D h_{fg} Y \rho_{mc} \frac{\partial^2 w_{mc}}{\partial z^2} \\
& + D Y h_{fg} \rho_{mc} \frac{\partial^2 w_{mc}}{R_f^2 \partial \theta^2} + D h_{fg} \rho_{mc} \frac{(w_{void} - w_{mc})}{ef/2} \\
& + h_{c(s-a)} (T_{skin} - T_{mc}) + h_{c(o-a)} (T_o - T_{mc}) \\
& + k Y \rho_a \frac{\partial^2 T_{mc}}{\partial z^2} + k Y \rho_{mc} \frac{\partial^2 T_{mc}}{R_f^2 \partial \theta^2} \\
& + k \rho_{mc} \frac{(T_{void} - T_{mc})}{ef/2} = 0
\end{aligned} \quad (1c)$$

where $h_{c(s-a)}$ is the convection coefficient of heat transfer between skin and air, $h_{c(o-a)}$ is the convection coefficient of heat transfer between the outer node fabric and air, T_{mc} is the air layer temperature, T_{skin} is the skin temperature, and T_o is the outer air node temperature.

The water vapor mass and energy balances in the fabric void node, outer node, and inner node are adapted from Ghali et al.'s model²³ and their derivation

can be found in the published work.^{5,9,23} The coupling to the fabric model leads to six equations for the fabric and air void nodes in terms for P_{v-void} , P_{v-o} , P_{v-i} , which is the partial pressure of the inner vapor pressure (kPa), and the temperatures of void node, inner fabric node, and our node, T_{void} , T_o , and T_i , respectively.

Mass and heat transport from the skin

In steady-state conditions, the inner cylinder representing the skin is uniformly heated at constant heat flux representing the segmental metabolic rate with wet skin condition, w_{skin} , corresponding to saturation pressure (P_{skin}) at skin temperature (T_{skin}). Therefore, the boundary condition at the inner cylinder (skin) is given by

$$\begin{aligned}
Q'' & = h_{m(s-a)} (P_{v-skin} - P_{v-mc}) + h_{c(s-a)} (T_{skin} - T_{mc}) \\
& + h_r (T_{skin} - T_o)
\end{aligned} \quad (2)$$

where Q'' is the metabolic rate (W/m^2).

In order to solve Equations (1) and (2) coupled to fabric nodes balances, a relation between the humidity ratio, the vapor pressure and the total pressure is needed. This relation is extracted from American Society of Heating, Refrigeration, and Air-Conditioning Engineers (ASHRAE) standards:²⁶

$$\begin{aligned}
w_{ma} & = 0.62198 \frac{P_{v-ma}}{P_{ma} - P_{v-ma}} \quad \text{or} \\
P_{v-ma} & = \frac{w_{ma} P_{ma}}{0.62198 + w_{ma}}
\end{aligned} \quad (3)$$

Boundary conditions

The thermal and pressure boundary conditions at the open apertures of the arm lower end and the trunk upper side are similar to those reported by Ismail et al.⁶ The main difference between this model and the previous unconnected model is that angular symmetry is no longer valid for the lower and upper arms (Z1, Z2), unlike the trunk (Z3). The cause of this asymmetry is the connection of the arm to the trunk, modeled as one large cylinder (Z4) where the flow is redistributed.

The physical model connectivity is shown in Figure 2 where (Z1) is considered as an open top and bottom annulus and the mass flow rate leaving (Z1) enters (Z2). At the end of the lower arm (Z1), and because we do not know the direction of the flow, two boundary conditions are presented as follows.

- (i) If the flow is upward through the opening, the hand can be modeled as a cylinder; thus, the pressure of the adjacent layer is similar to the pressure around a solid given by

$$P_s^*(\theta) = P_a + \frac{1}{2} c_p(\theta) \rho V_w^2 \quad (4a)$$

where P_s^* is the adjacent layer pressure around the hand modeled as a cylinder, and a Gaussian fit to the pressure distribution for a cylinder in an air flow was used.²⁷ Therefore, the axial mass flow at the end of the lower arm (Z1) is

$$\begin{aligned} \dot{m}_{az}(z=0, \theta, Z1) \\ = -\frac{Y^2}{12\nu} \frac{(P_{mc}(z=0, \theta, Z1) - P_s^*(z=0, \theta, Z1))}{dz} \end{aligned} \quad (4b)$$

- (ii) If the flow is downward through the opening, the gradient of pressure is zero, since the flow is leaving the domain as follows:

$$\frac{dP_{mc}}{dz}(z=0, \theta, Z1) = 0 \quad (4c)$$

The thermal boundary condition is similar to the condition considered by the literature^{6,28} where the air layer annulus temperature at the bottom arm opening at zone Z1 is given by

$$T_{mc}(z=0, \theta, Z1) = T_a \quad (\text{if the flow is entering}) \quad (4d)$$

$$\text{and } \frac{dT_{mc}}{dz}(z=0, \theta, Z1) = 0 \quad (\text{if the flow is leaving}) \quad (4e)$$

The humidity ratio at the bottom arm opening at zone Z1:

$$w_{mc}(z=0, \theta, Z1) = w_a \quad (\text{if the flow is entering}) \quad (4f)$$

and

$$\frac{dw_{mc}}{dz}(z=0, \theta, Z1) = 0 \quad (\text{if the flow is leaving}) \quad (4g)$$

At the interface between the lower and upper arms (Z1 and Z2), we apply the continuity of the pressure, temperature, and vapor pressure. The zone Z2 is considered as an open top and bottom annulus where the mass flow rate leaving (Z1) enters (Z2) and the mass flow rate leaving (Z2) enters (Z4). Zone Z3 is considered as an open top and closed bottom cylinder where

the mass flow rate leaving (Z3) enters (Z4). At the bottom closed end of (Z3), the boundary conditions are

$$\begin{aligned} T_{mc}(z=0, \theta, Z3) &= T_{skin}; w_{mc}(z=0, \theta, Z3) \\ &= w_{skin}; \dot{m}_{az}(z=0, \theta, Z3) = 0 \end{aligned} \quad (5a)$$

Because of the symmetry of Z3, the model can be divided according to the symmetry axis shown in Figures 1 and 2. Thus, the boundary conditions associated with symmetry are

$$\dot{m}_{a\theta}(z, \theta = 0 \text{ or } \pi, Z3) = 0 \quad (5b)$$

The top end of upper arm annulus (Z2) is partially opened because of the under arm region where the temperature and the humidity ratio of the air layer are considered similar to the skin conditions. The zone Z4 is considered as open top and bottom cylinder, where the mass flow rate leaving Z2 and Z3 enters the bottom end, while the mass flow rate leaving from the top is subjected to a discharge coefficient because of the area change and the 90° bending.²⁹ The boundary conditions associated with the leaving mass flow rates are

$$\begin{aligned} \frac{dT_{mc}}{dz}(z=H_3, \theta, Z4) &= 0; \frac{dP_{mc}}{dz}(z=H_3, \theta, Z4) = 0; \\ \frac{dw_{mc}}{dz}(z=H_3, \theta, Z4) &= 0 \end{aligned} \quad (6)$$

Numerical solution of simplified model. The coupled pressure and energy equations of the clothed cylinder with associated boundary conditions are discretized using a finite volume methodology. Thus, the air layer zone is divided into $N_r \times N_z \times 3$ grids of size Δz and $R_f \Delta \theta$ with thickness Y . Central differencing is used for second-order terms in the air layer pressure and energy equations. To ensure a grid-independent solution and accurate resolution, the numerical solution is repeated for different grid sizes. In the presented simulations, the number of grid points is 100 grids for both Z1 and Z2 zones, 200 grids for Z3, and 40 grids for Z4, with a maximum $\Delta \theta$ of 1°.

Computational fluid dynamics simulation of the upper clothed human body

In order to validate the air flow characteristics, including the temperature, pressure, and velocity direction and magnitude profiles at isothermal condition for the inner cylinder, a 3D detailed CFD model was developed using the commercial ANSYS Fluent 14.5 software.¹⁴ The flow is considered laminar, the air is considered as an ideal gas, and the porous media is

considered as a porous jump boundary condition where the hydraulic permeability is given as an input to the model.

CFD solves the governing equations for mass, momentum, and heat transfer in fluids.^{30,31} The simulations predict the flow velocity, temperature, and pressure field. To simulate air annuli of the clothed trunk and arms, a computational domain has been developed using geometry and grid generation tools and utilizing symmetry to reduce domain size. To mimic the human trunk and arm, two simple cylinders clothed with 0.001 m thickness fabric layer are constructed. In order to mimic the shoulder, a small channel of 7 cm length covered with fabric relates the large diameter cylinder to the small diameter cylinder. In order to be consistent with the human body model, the lower body part is constructed as a large clothed cylinder extended from the trunk and having the same boundary conditions (skin temperature). The geometrical dimensions of the upper human body and the jacket used in CFD are presented in Table 1. The upper clothed human body part is placed in a relatively large room where the wall facing the geometry permits the inlet flow at wind speed of 0.9 m/s (wind condition). The geometrical dimensions of the upper human body and the jacket³ of 65 cm height used in CFD are presented in Table 1.

Figure 3(a) shows the geometry drawn before generating the mesh. Figure 3(b) shows the half of the geometry in the half of the room that has to be meshed. The computational mesh generated uses approximately 1.92 million nodes where small elements (1 mm size) are used for the air gap adjacent to the human skin. The clothing is modeled as a porous jump boundary condition for the outer cylinders. In laminar flows, the pressure drop across the thin porous layer is typically proportional to velocity. Thus, by ignoring convective acceleration and diffusion, the porous model then reduces to Darcy's law given by

$$\nabla p = \frac{-\mu}{\gamma} \vec{v} \quad (7)$$

Table 1. Basic dimensions of the upper human body and the jacket

Segment	Circumference				
	Bust cm	Waist cm	Hip cm	Neck line cm	Cuff cm
Human body size	93	74	93	35	11
Jacket size ³	120	110	116	38	14

where γ is now the hydraulic permeability of the clothing in m^2 ; v is the velocity normal to the porous face; and ∇p is the gradient of pressure over the finite thickness.

The inputs required for the porous jump model are as follows:

- (i) identify the porous jump zone;
- (ii) set the hydraulic face permeability of the medium (γ in Equation (7));
- (iii) set the porous medium thickness.

In order to define the hydraulic face permeability γ (m^2), the air permeability α (m/s) is used as the velocity v that is normal to the porous face, and ∇p is substituted by the standard pressure change over the fabric thickness.

Results and discussion

This section focuses on the validation of the simulation results. The strategy of the validation consists of validating the flow characteristics with the CFD simulation at constant cross-wind. Then the total ventilation obtained from the connected ventilation of trunk and arm segments will be compared with published experimental data for cases of connected segments and isolated segments. A parametric study then follows to identify the parameters that induce high inter-segmental ventilation.

CFD validation

In order to validate the simplified model results, we first study the microclimate flow direction as well as the temperature distribution in the axial and angular directions of the air layer in the trunk and arm.

Flow direction validation. It is of interest to validate the direction of the flow at the connection between the clothed arm and trunk. Indeed, the connection of the microclimate zones of the different segments allows the air to be exchanged between them; therefore, when air flows from the microclimate of zone Z4 to that of Z2, supplementary air is forced to enter zone Z4 to conserve mass. This supplementary air will either come from the opening of aperture Z4 or through normal clothing ventilation, thus enhancing the segmental ventilation. However, this would result in a decrease in ventilation of the microclimate zone Z2, because air flowing from zone Z4 to Z2 is hotter than air coming from ambient conditions. This in turn forces microclimate air to flow out from zone Z2. Therefore, some air mass flow rate passes from zone Z2 downward to zone Z1 and leaves from the bottom opening or through

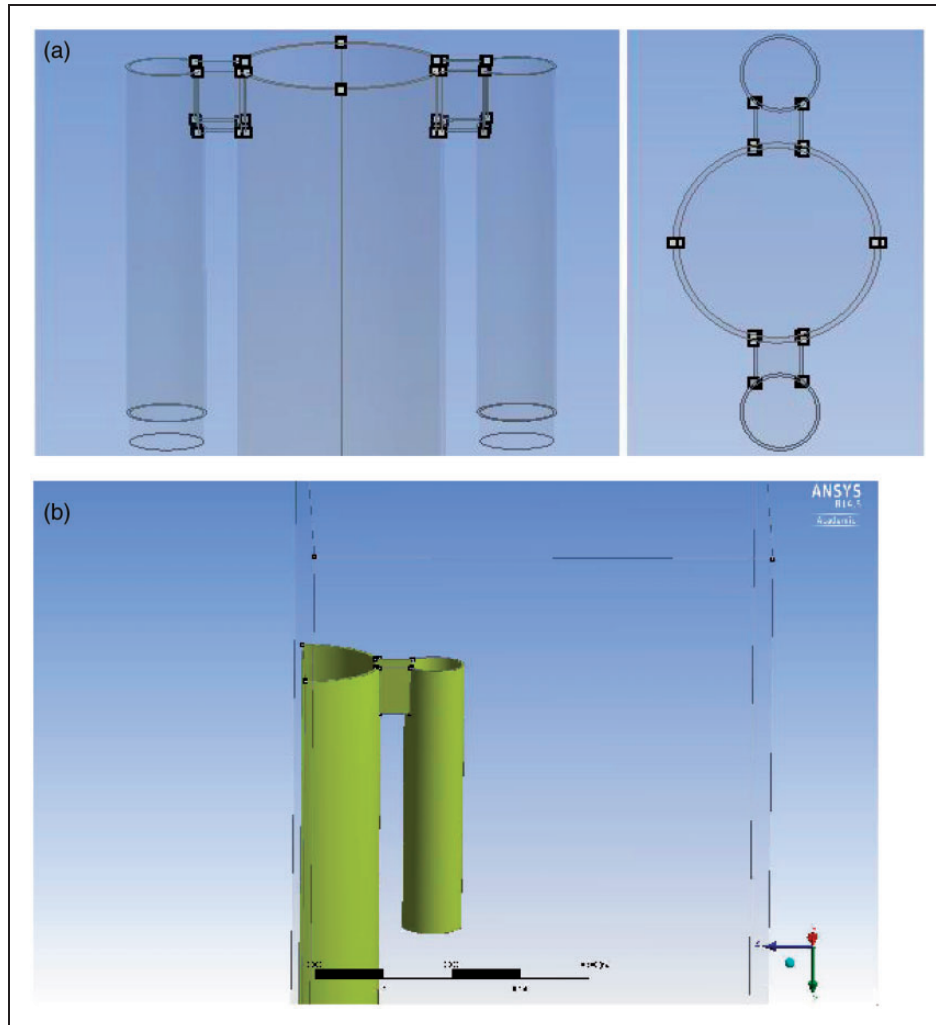


Figure 3. Plots of (a) front and top view of the upper human body and (b) symmetrical part of the domain that was simulated by ANSYS.

clothing. Ke et al.¹ pointed out this exchange phenomenon; however, they ignored its effect on ventilation by closing the garment connection during experiments. Therefore, to highlight the effect of the exchange rate between segments on their local ventilation values, the direction of the flow should be determined correctly.

The CFD simulation results of flow leaving the trunk top aperture, flow entering or leaving from the sleeve bottom aperture, and the flow in the connection between clothed trunk and arm are shown in Figures 4(a)–(c), respectively at $V_w=0.9$ m/s and $T_a=20^\circ\text{C}$. Figure 4(a) shows that the air leaves from the open top trunk upward. Figure 4(b) shows that the connection between the trunk and the arm by the shoulder segment allowed the flow to move from the trunk microclimate air to the arm microclimate air. Since the flow is transferred from the trunk to the arm, some air mass flow rate is leaving from the

microclimate air layer of the clothed arm to conserve the mass; this is shown in Figure 4(c).

In order to validate the velocity field (flow direction and velocity magnitude), simulations on the simplified ventilation model at the same conditions are conducted. The upper human body of the same geometries presented in Table 1 is simulated at $V_w=0.9$ m/s and $T_a=20^\circ\text{C}$ and at a segmental air gaps that are approximately estimated by subtracting the jacket circumference size from the human body size divided by 2π . The validation is shown in the corresponding Figures 5(a)–(c). Good agreement is shown between the CFD simulations and the simplified model with an error that does not exceed 14%.

The effect of the flow direction from the trunk to the arms is shown in Figure 6 where the distribution of the pressure over the trunk and over the arm is presented. Clearly, the pressure at the trunk air layer was

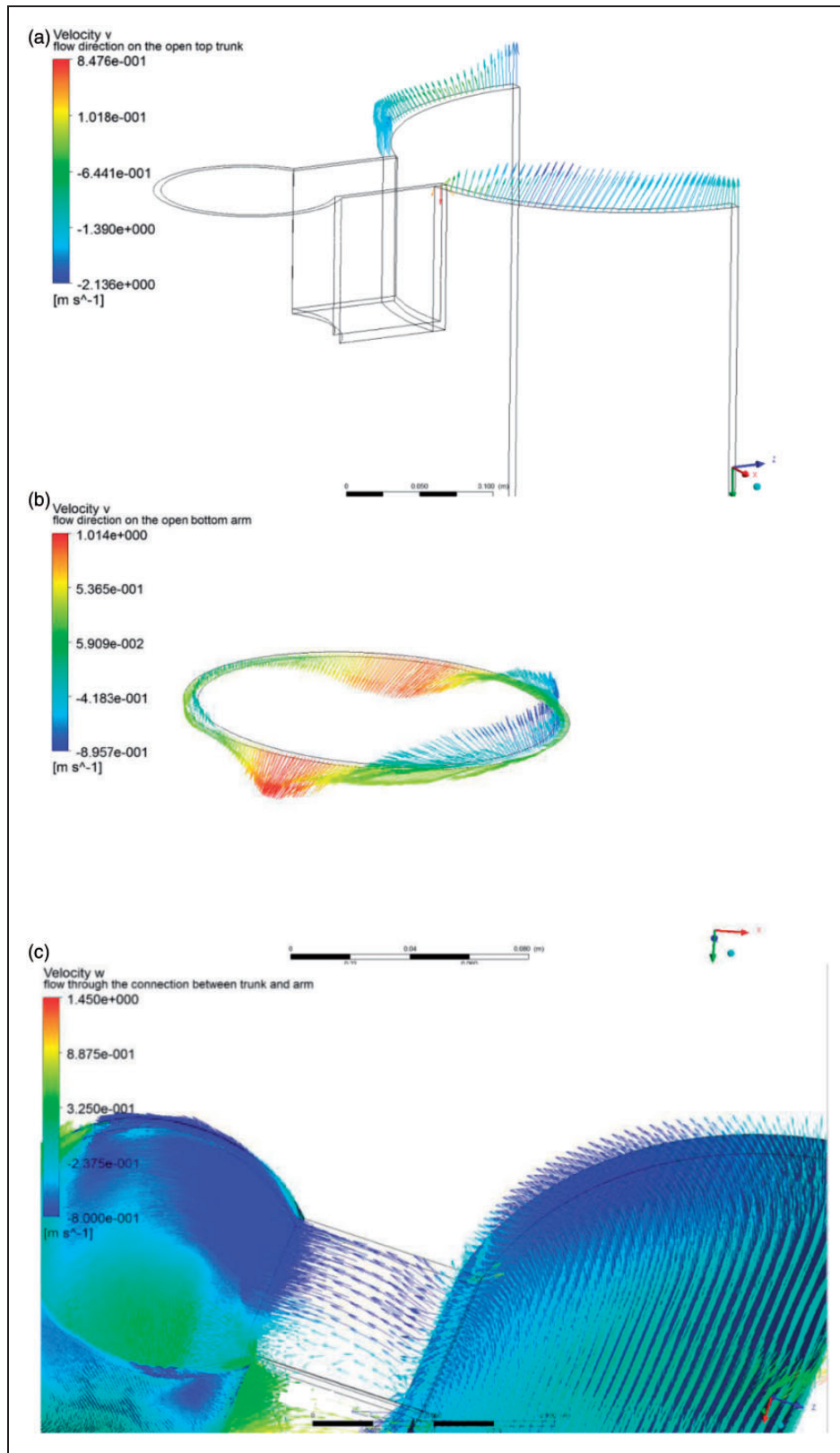


Figure 4. Computational fluid dynamics simulation plots of the flow (a) leaving the open top of clothed trunk and (b) leaving and entering the open bottom clothed arm (c) through the connection.

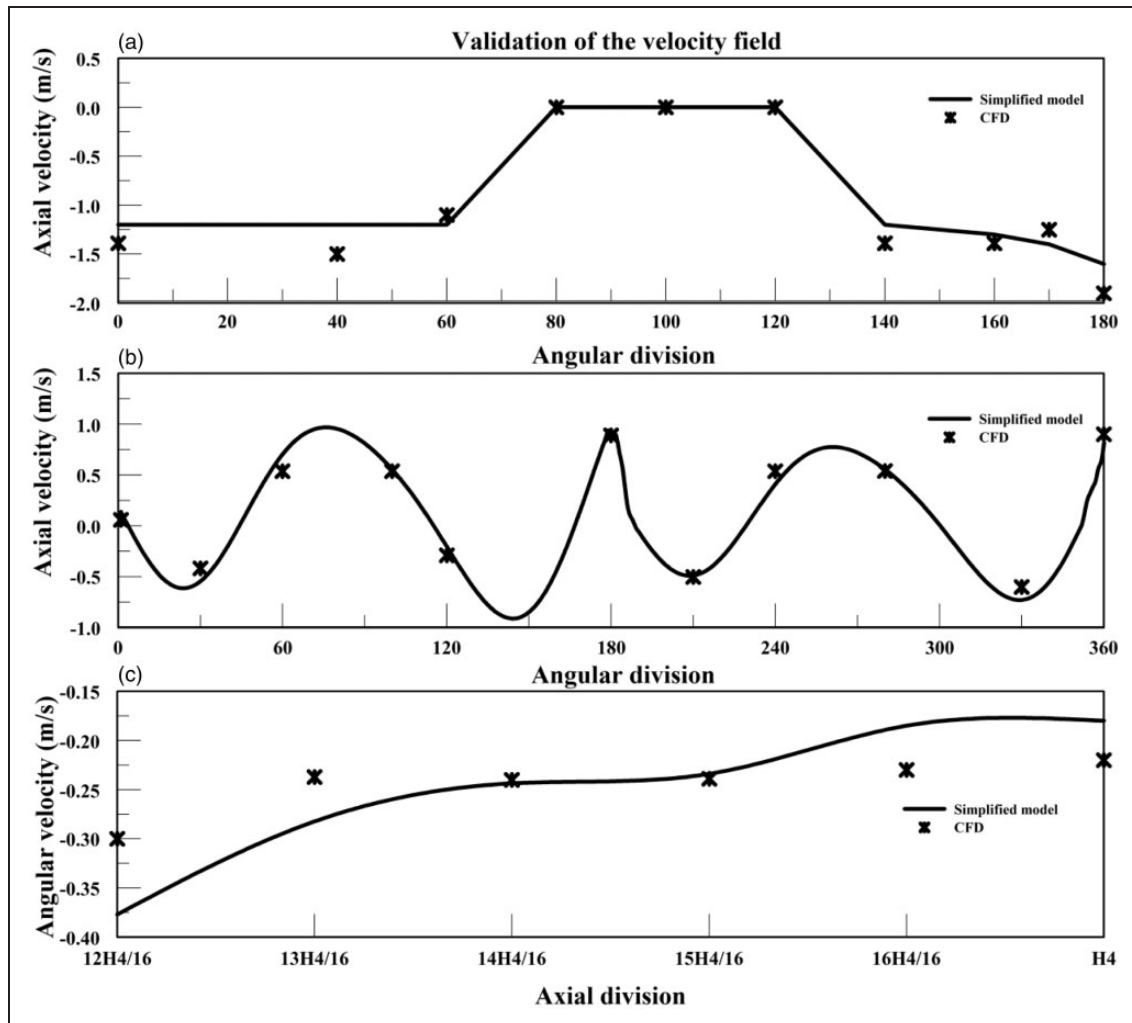


Figure 5. Validation of the velocity field (a) leaving the open top of clothed trunk and (b) leaving and entering the open bottom clothed arm (c) through the connection.

greater than that of the arm forcing the flow to move from the trunk to the arm. In addition, the pressure at the opening bottom end of the arm was negative and positive relative to ambient pressure. For this reason, some of this flow in the arm clothing annulus is lifted up and some of this flow is pushed down (see Figure 4(b)). Finally, the positive pressure of the upper part of the trunk illustrates clearly the upward flow of the opening at the top end of the trunk.

Temperature validation. Figures 7(a)–(d) show the variation of the model predicted temperature in the microclimate air layers of four zones (Z1, Z2, Z2, Z4) and corresponding averaged valued calculated by the CFD model at $V_w = 0.9$ m/s and $T_a = 20^\circ\text{C}$.

Figure 7(a) shows the variation of the angular-averaged temperature in the axial direction of the lower clothed arm (Z1) versus its height H1. The temperature

increased from the ambient temperature at the bottom opening, as expected due to the warm skin. Figure 7(b) shows the validation of the angular-averaged temperature in the axial direction for the upper clothed arm versus its height H_2 . The temperature was also found to increase because of two factors: (i) Z2 is connected to Z4 where the top end is partially closed; and (ii) the top end of Z2 is connected to the clothed trunk where the microclimate air layer is closed (the under arm region). Figure 7(c) shows the validation of the angular-averaged temperature of the microclimate trunk (Z3) versus its height H_3 . The temperature decreased from the skin condition at the closed bottom end. The increase in the angular-average temperature at the top end of zone Z3 was also due to the skin temperature under the arm. Figure 7(d) shows the validation of the angular-averaged temperature of the connection zone (Z4) versus its height H_4 . The temperature increases axially because

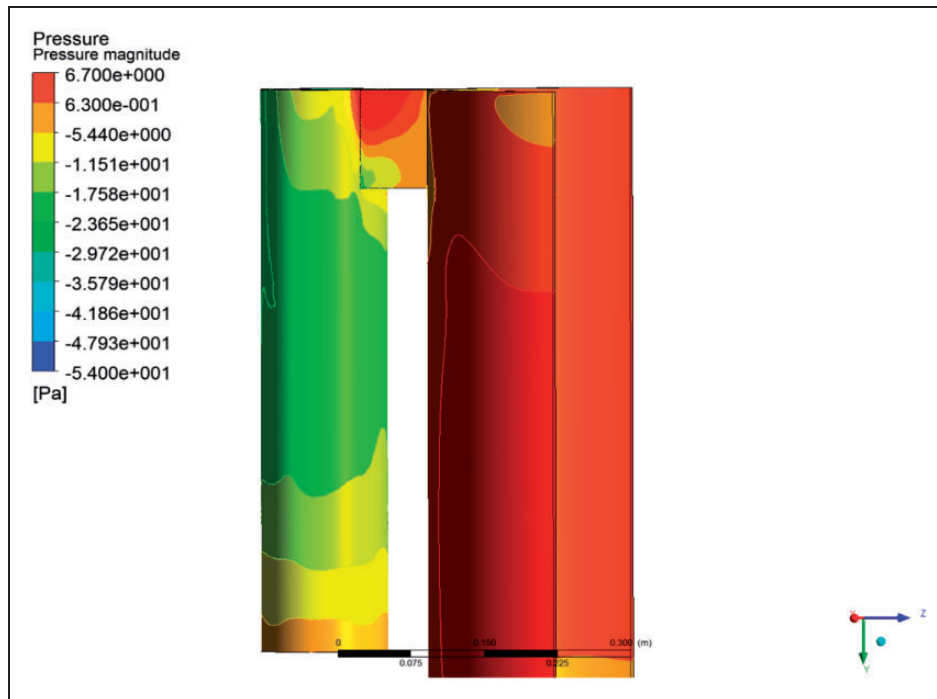


Figure 6. Distribution of the relative pressure obtained from computational fluid dynamics simulation.

the top end was partially closed where the skin conditions were applied at the closed part and zero-gradient was applied at the open part.

Model validation with published experimental data

The mathematical ventilation model developed in this study elaborates the effect of connection on the overall ventilation. The aim of this section is to validate the overall ventilation rates through a permeable jacket ($\alpha = 0.135$ m/s) at different wind velocities with the published experiment³ where the connection between segments is left open to allow the air exchange between them. Furthermore, the segmental ventilation rates computed with opened connection condition are compared with the segmental ventilation rates computed with closed connection condition (independent cylinders). This comparison will show up the effect of connections on varying the ventilation rates and the necessity to include their effects in order to approach more accurately the experimental values of ventilation rates.

Ke et al.³ used a steady-state tracer gas method for measuring the microclimate ventilation rates. Nitrogen (N_2) was chosen as the tracer gas. Three wind speeds were used: $V_w \leq 0.1$ m/s (no wind), $V_w = 0.6$ m/s, and $V_w = 0.9$ m/s. The experiment was carried out on a

standing shop manikin in an air-conditioned chamber at 20°C ambient temperature and $40\% \pm 10\%$ relative humidity. The dimensions used in the published experiment³ (garment S1) are the same as those used in the model. Table 2 shows the total ventilation values predicted by the connected model as compared with the published experimental values at different wind speeds for the same permeable jacket when the connection effect is included and when it is excluded. It is observed that the connected model is closer in accuracy to the published experiment (with an error not exceeding 12%) than the unconnected one (with an error exceeding 15%) at relatively high wind speeds ($V_w \geq 0.6$ m/s). However, it shows approximately the same result at low wind speeds ($V_w \leq 0.1$ m/s).

Another validation is performed comparing overall ventilation to measured values published in a recent experiment by Ke et al.¹⁵ on a thermal manikin heated at $T_{skin} = 35^\circ\text{C}$ in an environment at 20°C and 50% relative humidity. Two wind speeds were used: $V_w \leq 0.3$ m/s (here we assumed it to be 0.3 m/s) and $V_w = 1.1$ m/s with the connections between segments kept open. Table 3 shows the total ventilation values predicted by the connected model (summing up the local ventilation of the trunk and arms) as compared with the published experimental values at two different wind speeds for the garment G1 of 0.135 m/s permeability. Good agreement is found between the

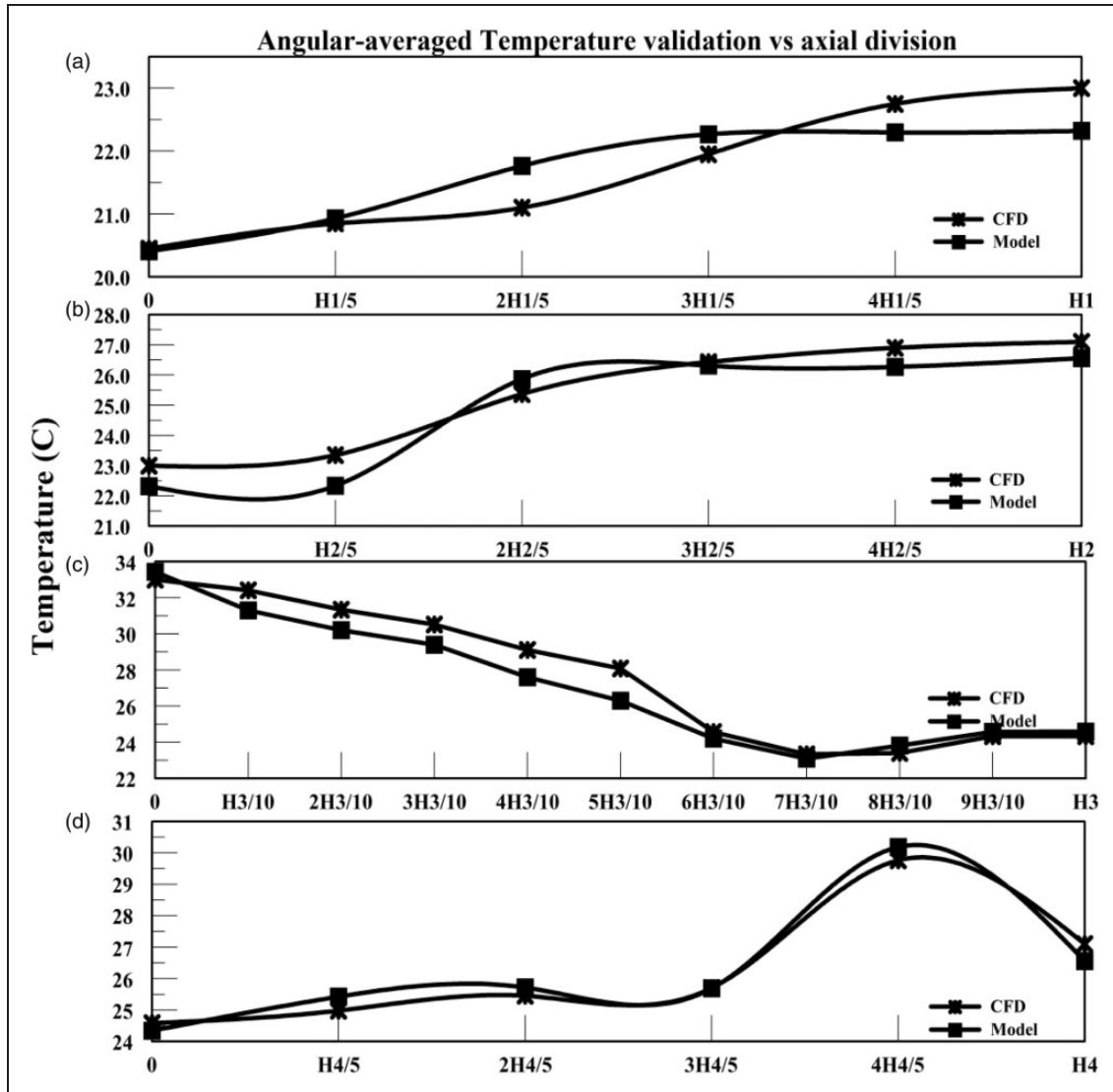


Figure 7. Angular-averaged axial temperature validation obtained from the ventilation model at (a) zone Z1, (b) at zone Z2, (c) at zone Z3, and (d) at zone Z4.

Table 2. Validation of the model ventilation at different wind speeds

V_w (m/s)	0.1		0.6		0.9	
Experiment ventilation ³ (l/min)	36.57		44.5		58.5	
	Ventilation (l/m)	Relative error (%)	Ventilation (l/m)	Relative error (%)	Ventilation (l/m)	Relative error (%)
Model connected (l/min)	32.12	12.16	40.65	8.65	60.01	2.58
Model unconnected (l/min)	32.54	11.02	37.79	15.07	55.09	5.82

Table 3. Validation of the model ventilation at different wind speeds

	$V_a = 0.3$ m/s	$V_a = 1.1$ m/s
Experiment ventilation ³ (l/min)	55.27 ± 6.6	82.73 ± 7.79
Model connected (l/min)	48.12	75.1

connected mathematical model and the published experiment, as the predicted values fall within the experimental error ranges provided in the published work.¹⁵

Parametric study

In order to understand the effect of connection on the ventilation rate, it is of interest to isolate the new parameter, the inter-segmental ventilation, and compute its value under different flow conditions and for different physical and geometric clothing parameters. The inter-segmental ventilation is defined as the air mass flow rate (l/min) that flows from the trunk to the arm. This parameter is important because of its impact in varying the segmental ventilation of the trunk and the arm. In the case of the flow of air from the trunk to the arm, the air will enter the trunk air layer from the ambient conditions through clothing and will leave through the arm connection, or the clothing, or the top opening. This will cause an increase of trunk ventilation and a decrease of arm ventilation, because the air that enters the arm microclimate is heated and is hotter than the ambient air. The developed model predicts the net mass flow rate (l/min) leaving the trunk and entering the arm. However, different factors influence the inter-segmental ventilation and these parameters include wind speed, clothing permeability, and clothing apertures. Note that the non-uniformity in microclimate gap size due to wind pressure at the front compared to the back is not included in these parameters due to the assumption of fully developed flow in the axial and in angular directions. However, we simulated the case of non-uniform Y by choosing its value at the front to be 50% of that of Y at the back while keeping Y constant in the Z direction to see if there is any significant influence on inter-segmental ventilation. It was found that the change in inter-segmental ventilation was less than 2%. In order to study the impact of these different factors on the inter-segmental ventilation, we assume that the inter-segmental ventilation is positive if the flow of air is from the trunk to the arm and negative vice versa.

Figure 8(a) shows the inter-segmental ventilation using a permeable jacket ($\alpha = 0.135$ m/s) at different

wind speeds. It was shown that when the velocity increases, the inter-segmental ventilation increased. At low wind speeds ($V_w \leq 0.1$ m/s), it was found that the inter-segmental ventilation was no longer significant. In this case, the trunk and the arm can be modeled as independent segments. However, at high wind speeds ($V_w \geq 0.9$ m/s), the inter-segmental ventilation exceeds 5 l/min. Another important factor that affects the inter-segmental ventilation is the clothing permeability. In general, the jacket permeability allows air to enter the segmental microclimate air layers and the interconnection allows the air exchange between the segments. In order to study the impact of permeability on the inter-segmental ventilation, different jacket permeabilities are investigated at a wind speed of 1 m/s. Figure 8(b) illustrated this impact. It was shown that at relatively high permeability ($\alpha = 0.135$ m/s), the inter-segmental ventilation was significant and reaches 5 l/min. However, at lower permeability ($\alpha = 0.05$ m/s), the connection impact vanished and the air exchange between the trunk and the arm was no longer important. The third important parameter that affects the inter-segmental ventilation is the opening at the bottom end of the lower arm and at the neck. Figure 8(c) illustrated this effect by estimating the inter-segmental ventilation at different apertures. At $V_w = 1$ m/s and for a permeable jacket ($\alpha = 0.135$ m/s), it was found that the inter-segmental ventilation became more significant when the bottom opening of the arm was open than when it was closed. This is because the pressure at the arm microclimate air layer increases when the bottom end of the arm is closed. This pressure increase caused lower air exchange leaving the trunk to the arm. However, this was not the case when the top end of the trunk was closed. There was no significant variation in the inter-segmental ventilation in both cases: open top end or closed top end.

As discussed earlier, the inter-segmental ventilation causes the trunk ventilation to increase by allowing some fresh air mass flow rate to penetrate instead of the heated mass flow rate (inter-segmental ventilation). Indeed, the trunk ventilation is essential in providing human comfort.³² It is considered as the most influential segment because of its highest segmental heat loss.³³ Several studies have reported the trunk influence on the segmental and overall thermal sensation.^{34,35}

Table 4 summarizes the trunk ventilation increase at different conditions. It was observed that the inter-connection provided an important role in increasing the trunk ventilation by more than 15% at high wind speeds ($V_w \geq 0.9$ m/s), relatively high permeability ($\alpha = 0.135$ m/s), and open bottom arm apertures. On the other hand, the heated air mass flow rate that

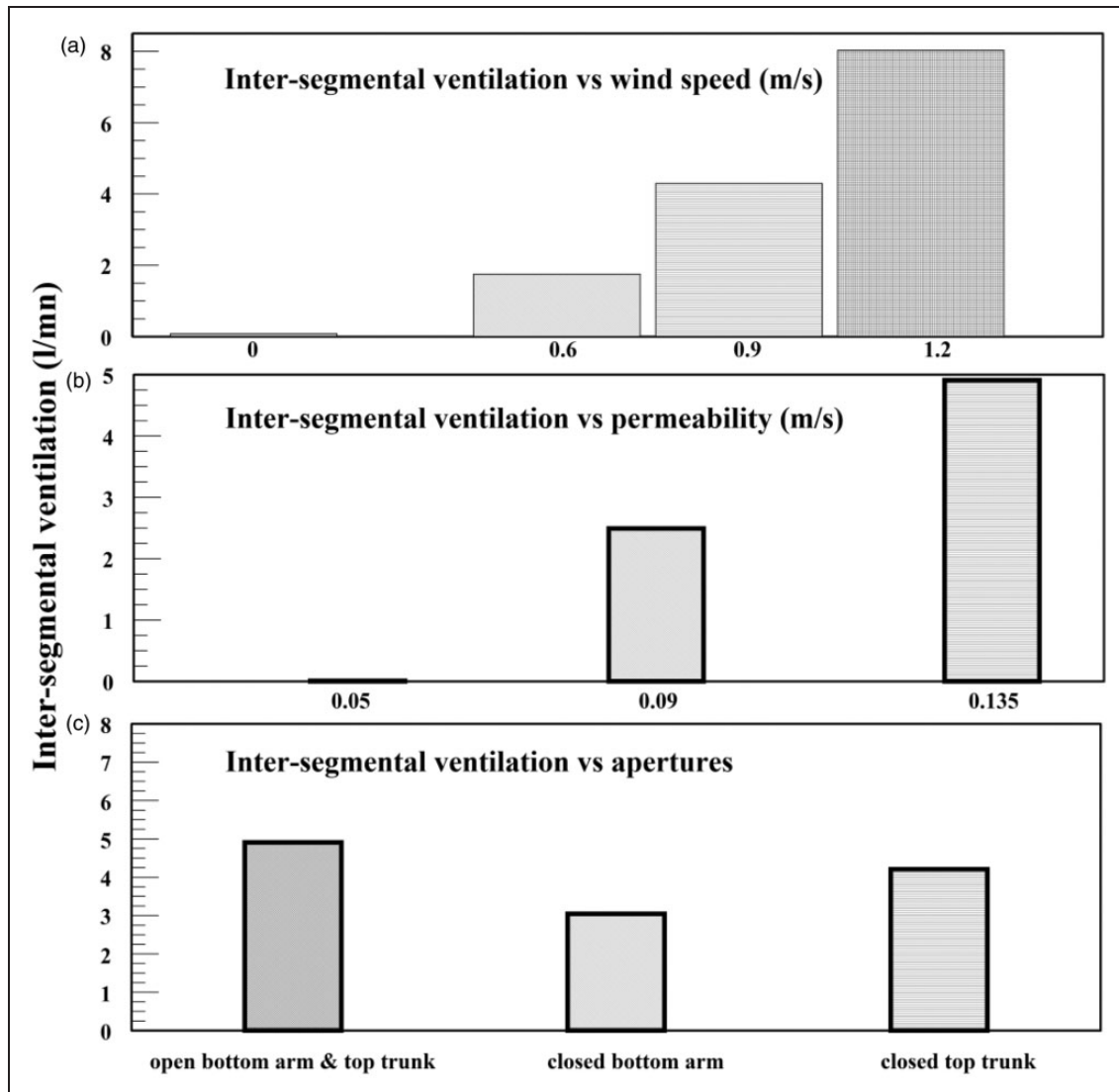


Figure 8. Estimation of the inter-segmental ventilation obtained from the ventilation model as a function of (a) wind speed, (b) permeability, and (c) apertures.

enters the arm microclimate layer causes a decrease in the arm ventilation.

Table 5 summarizes the arm ventilation reduction when considering the connected segments. It was shown that that the inter-connection provided a reduction in the arm ventilation by more than 5% at high wind speeds ($V_w \geq 0.9$ m/s), relatively high permeability ($\alpha = 0.135$ m/s), and open bottom arm apertures.

The developed simplified model and the inter-segmental ventilation behavior may be used in the design of protective clothing where improved ventilation of the human trunk is needed, which can be achieved by increasing inter-segmental ventilation from the trunk to the arm through the connection.

Conclusion

In order to find the effect of connection on the ventilation rate, a sound mathematical model is developed of the air flow in the microclimate air layer between the clothing and the upper human body part. The connection between the clothed trunk and the arm microclimate air layers allowed the air to be exchanged between the segments. It was found that at relatively high wind speed ($V_w \geq 0.9$ m/s) and permeable jacket (0.135 m/s), air flowed from the trunk to the arm microclimate air layer. The heated air mass flow rate leaving the trunk was replaced by fresh air at ambient conditions, which increased the local ventilation rate of the trunk. The model was validated by 3D CFD simulations. Good

Table 4. Percentage increase of trunk ventilation at different conditions

	Trunk connected (l/min)	Trunk unconnected (l/min)	Increase (%)
$V_w = 0.1 \text{ m/s}$; $\alpha = 0.135 \text{ m/s}$	1.04	1.04	0.40
Open bottom & open top			
$V_w = 0.6 \text{ m/s}$; $\alpha = 0.135 \text{ m/s}$	15.17	13.22	14.73
Open bottom & open top			
$V_w = 0.9 \text{ m/s}$; $\alpha = 0.135 \text{ m/s}$	35.83	31.06	15.35
Open bottom & open top			
$V_w = 1.2 \text{ m/s}$; $\alpha = 0.135 \text{ m/s}$	63.69	54.77	16.28
Open bottom & open top			
$V_w = 1.0 \text{ m/s}$; $\alpha = 0.05 \text{ m/s}$	16.39	16.38	0.06
Open bottom & open top			
$V_w = 1.0 \text{ m/s}$; $\alpha = 0.09 \text{ m/s}$	29.50	26.60	10.90
Open bottom & open top			
$V_w = 1.0 \text{ m/s}$; $\alpha = 0.135 \text{ m/s}$	44.23	38.46	15.02
Open bottom & open top			
$V_w = 1.0 \text{ m/s}$; $\alpha = 0.135 \text{ m/s}$	42.05	38.46	9.32
Closed bottom & open top			
$V_w = 1.0 \text{ m/s}$; $\alpha = 0.135 \text{ m/s}$	43.82	38.18	14.79
Open bottom & closed top			

Table 5. Percentage change of arm ventilation at different conditions

	Arm connected (l/min)	Arm unconnected (l/min)	Decrease (%)
$V_w = 0.1 \text{ m/s}$; $\alpha = 0.135 \text{ m/s}$	16.37	16.62	1.50
Open bottom & open top			
$V_w = 0.6 \text{ m/s}$; $\alpha = 0.135 \text{ m/s}$	13.1	13.53	3.17
Open bottom & open top			
$V_w = 0.9 \text{ m/s}$; $\alpha = 0.135 \text{ m/s}$	12.21	12.63	3.32
Open bottom & open top			
$V_w = 1.2 \text{ m/s}$; $\alpha = 0.135 \text{ m/s}$	15.35	17.34	11.47
Open bottom & open top			
$V_w = 1.0 \text{ m/s}$; $\alpha = 0.05 \text{ m/s}$	8.00	8.32	3.84
Open bottom & open top			
$V_w = 1.0 \text{ m/s}$; $\alpha = 0.09 \text{ m/s}$	10.89	11.38	4.30
Open bottom & open top			
$V_w = 1.0 \text{ m/s}$; $\alpha = 0.135 \text{ m/s}$	12.94	13.59	4.78
Open bottom & open top			
$V_w = 1.0 \text{ m/s}$; $\alpha = 0.135 \text{ m/s}$	13.36	13.85	3.53
Closed bottom & open top			
$V_w = 1.0 \text{ m/s}$; $\alpha = 0.135 \text{ m/s}$	13.24	13.59	2.57
Open bottom & closed top			

agreement is found between the CFD simulation results of ventilation rate and angular and axial averaged temperature distributions in the air layers of trunk and arms segments with values predicted by our simplified model. The predicted overall ventilation rates were found to be more accurate and closer to published experimental data when the effect of connection was included.

Using the validated model in a parametric study, it was also found that at relatively high wind speed, high jacket permeability, and open bottom arm, the inter-segmental ventilation was maximal.

Funding

This work was supported by the Lebanese National Council for Scientific Research (CNRS).

References

- Ke Y, Li J and Havenith G. An improved experimental method for local clothing ventilation measurement. *Int J Ind Ergon* 2014; 44: 75–81.
- Bouskill L, Havenith G, Kuklane K, et al. Relationship between clothing ventilation and thermal insulation. *AIHA J* 2002; 63:262–268.
- Ke Y, Havenith G, Li J, et al. A new experimental study of influence of fabric permeability, clothing sizes, openings and wind on regional ventilation rates. *Fibers Polym* 2013; 14: 1906–1911.
- Havenith G, Zhang P, Hatcher K, et al. Comparison of two tracer gas dilution methods for the determination of clothing ventilation and of vapour resistance. *Ergonomics* 2014; 53: 548–558.
- Ghaddar N and Ghali K. Effect of moisture transport on mixed convection in vertical annulus of a heated clothed vertical wet cylinder in uniform cross wind In: *14th international heat transfer conference* Washington, DC, 2010.
- Ismail N, Ghaddar N and Ghali K. Predicting segmental and overall ventilation of ensembles using an integrated bioheat and clothed cylinder ventilation models. *Text Res J* 2014; 84: 2198–2213.
- Ghaddar N, Ghali K and Jreije B. Ventilation of wind-permeable clothed cylinder subject to periodic swinging motion: Modeling and experimentation. *J Heat Transfer* 2008; 130: 1107–2020.
- Kind R, Jenkins J and Seddigh F. Experimental investigation of heat transfer through wind-permeable clothing. *Cold Region Sci Technol* 1991; 20: 39–49.
- Ghali K, Othmani M, Jreije B, et al. Simplified heat transport model of a wind-permeable clothed cylinder subject to swinging motion. *Text Res J* 2009; 79: 1043–1055.
- Ghaddar N, Ghali K, Harathani J, et al. Ventilation rates of microclimate air annulus of the clothing skin system under periodic motion. *Int J Heat Mass Transfer* 2005; 48: 3151–3166.
- Ghaddar N, Ghali K and Chehaitly S. Assessing thermal comfort of active people in transitional spaces in presence of air movement. *Energy Build* 2011; 43: 2832–2842.

12. Al-Othmani M, Holmer I, Kuklane K, et al. Experimental and theoretical study of ventilation and heat loss from isothermally heated clothed vertical cylinder in uniform flow field. *J Appl Mech* 2010; 77: 031011–8.
13. Leong J and Lai F. Natural convection in a concentric annulus with a porous sleeve. *Int J Heat Mass Transfer* 2006; 49: 3016–3027.
14. ANSYS Software. ANSYS Inc., Southpointe, 2600 ANSYS Drive, Canonsburg, PA15317, USA.
15. Ke Y, Havenith G, Zhang X, et al. Effects of wind and clothing apertures on local clothing ventilation rates and thermal insulation. *Text Res J* 2014; 84: 941–952.
16. Alam M, Moriya M, Takai K, et al. Fluctuating fluid forces acting on two circular cylinders in a tandem arrangement at a subcritical Reynolds number. *J Wind Eng Ind Aerod* 2003; 91: 139–154.
17. Xu S, Zhou Y and So R. Reynolds number effects on the flow structure behind two side-by-side cylinders. *Phys Fluids* 2003; 15: 1214–1219.
18. Bearman PW. The effect of base bleed on the flow behind a two-dimensional model with a blunt trailing edge. *Aeronaut Q* 1967; 18: 207–224.
19. Wood C. Visualization of an incompressible wake with base bleed. *J Fluid Mech* 1967; 29: 259–272.
20. Ko N, Wong P and Leung R. Interaction of flow structures within bistable flow behind two circular cylinders of different diameters. *Exp Therm Fluid Sci* 1996; 12: 33–44.
21. Gao Y, Etienne S, Wang X, et al. Experimental study on the flow around two tandem cylinders with unequal diameters. *J Ocean Univ* 2014; 13: 761–770.
22. Zhao M. and Yan G. Numerical simulation of vortex-induced vibration of two circular cylinders of different diameters at low Reynolds number. *Physics of fluids* 2013; 25(8): 083601.
23. Ghali K, Ghaddar N and Jones B. Empirical evaluation of convective heat and moisture transport coefficients in porous cotton medium. *ASME Heat Transfer J* 2002; 124: 530–537.
24. Ghaddar N, Ghali K and Harathani J. Modulated air layer heat and moisture transport by ventilation and diffusion from clothing with open aperture. *J Heat Transfer* 2005; 127: 287–297.
25. Chaves C, Camargo J and Correa V. Combined forced and free convection heat transfer in a semi-porous open cavity. *Sci Res Essay* 2008; 3: 332–337.
26. ASHRAE. *ASHRAE handbook-fundamentals*. Atlanta, GA: ASHRAE, 1997.
27. Stuart ID. Wind induced transfer of water vapor and heat through clothing. *Text Res J* 1987; 57: 247–256.
28. Anil LS and Reji C. Numerical prediction of natural convection in vented cavities using restricted domain approach. *Int J Heat Mass Transfer* 2009; 52: 724–734.
29. Malone T and Parr AD. Bend losses in rectangular culverts. Report No. K-TRAN: KU-05-5, Kansas State University and University of Kansas, Kansas, 2008.
30. Pletcher R, Tannehill JC and Anderson DA. *computational fluid mechanics and heat transfer*. Philadelphia, PA: Taylor & Francis, 1997.
31. Blazek J. *Computational fluid dynamics: Principles and applications*. 2nd ed. New York: Elsevier, 2005.
32. Nakamura M, Yoda T, Crawshaw L, et al. Regional differences in temperature sensation and thermal comfort in humans. *J Appl Physiol* 2008; 105: 1897–1906.
33. Caroline J and Havenith G. Body mapping of sweating patterns in male athletes in mild exercise-induced hyperthermia. *J Appl Physiol* 2011; 111: 1391–1404.
34. Ouzzahra Y, Havenith G and Redortier B. Regional distribution of thermal sensitivity to cold at rest and during mild exercise in males. *J Therm Biol* 2012; 37: 517–523.
35. Gerett N, Ouzzahra Y, Coleby S, et al. Thermal sensitivity to warmth during rest and exercise: a sex comparison. *Eur J Appl Physiol* 2014; 114: 1451–1462.

Nomenclature

Z1	Zone 1 (clothed lower arm)
Z2	Zone 2 (clothed upper arm)
Z3	Zone 3 (clothed trunk)
Z4	Zone 4 (clothed connection)
H ₁	Zone 1 height
H ₂	Zone 2 height
H ₃	Zone 3 height
H ₄	Zone 4 height
C _p	specific heat at constant pressure (J/kg K)
e _f	fabric thickness (m)
Y	air layer thickness (m)
g	gravitational acceleration (m/s ²)
h _{c(s-a)}	heat transfer coefficient from the skin to the trapped air layer (W/m ² ·K)
h _{c(o-a)}	heat transfer coefficient from the outer fabric node to the air layer (W/m ² ·K)
h _r	linearized radiative heat transfer (W/m ² ·K)
K	thermal conductivity of air (W/m·K)
D	air-to-air diffusivity (m ² /s)
Z	axial direction
R _f	fabric cylinder radius (m)
e _f	fabric thickness (m)
ṁ _{aY}	mass flow rate of air in the radial direction (kg/m ² ·s)
ṁ _{aθ}	mass flow rate of air in the angular direction (kg/m ² ·s)
ṁ _{aZ}	mass flow rate of air in the axial direction (kg/m ² ·s)
ṁ _a	total ventilation rate (kg/m ² ·s)
P _{mc}	pressure of the microclimate air (kPa)
P _s	pressure at the external surface of the fabric (kPa)
T _{mc}	temperature of the microclimate air (°C)
T _a	ambient temperature (°C)
T _{skin}	skin temperature (°C)
T _o	temperature of the fabric outer layer (°C)
T _i	temperature of the fabric outer layer (°C)
T _{void}	temperature of the fabric void layer (°C)
V _w	velocities of the environment cross-wind (m/s)

Q''	metabolic rate (W/m^2)	w_a	humidity ratio of the ambient air
Max	maximum	h_{fg}	heat of evaporation
ΔP_m	general pressure difference used to estimate permeability experimentally	$h_{m(o-a)}$	the mass transfer coefficient between outer fabric node and microclimate air
$h_{m(s-a)}$	the mass transfer coefficient between skin and microclimate air	v	the velocity of air through the fabric
P_{v-skin}	the partial pressure of the skin vapor pressure (kPa)	Greek symbols	
P_{v-mc}	the partial pressure of the microclimate air vapor pressure (kPa)	α	fabric air permeability ($\text{m}^3/\text{m}^2\cdot\text{s}$)
P_{v-o}	the partial pressure of the outer vapor pressure (kPa)	β	the volumetric thermal expansion ($^{\circ}\text{C}^{-1}$)
P_{v-void}	the partial pressure of the void vapor pressure (kPa)	γ	the hydraulic permeability in m^2
w_{void}	humidity ratio of the void node fabric	ν	kinematic viscosity of air (m^2/s)
w_{mc}	humidity ratio of the microclimate air	ρ_{ma}	density of air (kg/m^3)
		θ	angular coordinate